Research Article | Vol. 8, No. 4 | 1 Apr 2018 | OPTICAL MATERIALS EXPRESS 1075
Optical Materials EXPRESS

Axial InAs(Sb) inserts in selective-area InAsP nanowires on InP for optoelectronics beyond 2.5 µm

DINGKUN REN,[1,*] ALAN C. FARRELL,[1] AND DIANA L. HUFFAKER[1,2,3]

[1]*Department of Electrical and Computer Engineering, University of California at Los Angeles, Los Angeles, California 90095, USA*
[2]*California NanoSystems Institute, University of California at Los Angeles, Los Angeles, California 90095, USA*
[3]*School of Physics and Astronomy, Cardiff University, Cardiff, Wales CF24 3AA, UK*
**dingkun.ren@ucla.edu*

Abstract: In this work, we report on the growth of high yield small bandgap InAs and InAsSb inserts embedded in InAsP nanowires grown on an InP substrate by catalyst-free selective-area metal-organic chemical vapor deposition. It is observed that the growth of the inserts with high aspect ratios can be achieved by properly tuning the V/III ratio. Nanowire arrays with InAs(Sb) inserts exhibit strong photoluminescence at 77 K from interband transitions, spanning a wavelength range of 2.30–3.70 µm. In addition, the InAsP/InAs heterointerfaces are characterized by a scanning transmission electron microscope and an energy-dispersive X-ray spectroscopy. We believe that these results pave the way to engineering interband transitions and enabling hybrid integration for nanoscale optical devices at the mid-wavelength infrared.

OCIS codes: OCIS codes: (160.4236) Nanomaterials; (230.0250) Optoelectronics; (040.3060) Infrared.

References and links

1. C. Li, Y. Zhang, K. Wang, Y. Gu, H. Li, and Y. Li, "Distinction investigation of InGaAs photodetectors cutoff at 2.9 µm," Infrared Phys. Technol. **53**(3), 173–176 (2010).
2. G. Hasnain, B. F. Levine, D. L. Sivco, and A. Y. Cho, "Mid-infrared detectors in the 3–5 µm band using bound to continuum state absorption in InGaAs/InAlAs multiquantum well structures," Appl. Phys. Lett. **56**(8), 770–772 (1990).
3. B. Chen, W. Y. Jiang, J. Yuan, A. L. Holmes, Jr., and B. M. Onat, "Demonstration of a room-temperature InP-based photodetectors operating beyond 3µm," IEEE Photonics Technol. Lett. **23**(4), 218–220 (2011).
4. B. Chen, W. Jiang, J. Yuan, A. L. Holmes, Jr., and B. M. Onat, "SWIR/MWIR InP-based p-i-n photodiodes with InGaAs/GaAsSb type-II quantum wells," ," IEEE J. Quantum Electron. **47**(9), 1244–1250 (2011).
5. B. Chen and A. L. Holmes, Jr., "InP-based short-wave infrared and midwave infrared photodiodes using a novel type-II strain-compensated quantum well absorption region," Opt. Lett. **38**(15), 2750–2753 (2013).
6. B. Chen, "Active region design and gain characteristics of InP-based dilute bismide type-II quantum wells for mid-IR lasers," IEEE Trans. Electron Dev. **64**(4), 1606–1611 (2017).
7. S. R. Kurtz, A. A. Allerman, and R. M. Biefeld, "Midinfrared lasers and light-emitting diodes with InAsSb/InAsP strained-layer superlattice active regions," Appl. Phys. Lett. **70**(24), 3188–3190 (1997).
8. R. M. Biefeld, S. R. Kurtz, and A. A. Allerman, "The metal-organic chemical vapor deposition growth and properties of InAsSb mid-infrared (3–6-μm) lasers and LED's," IEEE J. Sel. Top. Quantum Electron. **3**(3), 739–748 (1997).
9. K. A. Dick and P. Caroff, "Metal-seeded growth of III-V semiconductor nanowires: towards gold-free synthesis," Nanoscale **6**(6), 3006–3021 (2014).
10. D. Ren, A. C. Farrell, B. S. Williams, and D. L. Huffaker, "Seeding layer assisted selective-area growth of As-rich InAsP nanowires on InP substrates," Nanoscale **9**(24), 8220–8228 (2017).
11. A. Behres, D. Püttjer, and K. Heime, "Low-pressure metal organic vapour-phase epitaxy and characterization of strained InAs(P)/InAsSb superlattices for infrared emitters," J. Cryst. Growth **195**(1–4), 373–377 (1998).
12. B. Lane, Z. Wu, A. Stein, J. Diaz, and M. Razeghi, "InAsSb/InAsP strained-layer superlattice injection lasers operation at 4.0 μm grown by metal-organic chemical vapor deposition," Appl. Phys. Lett. **74**(23), 3438–3440 (1999).
13. P. Christol, M. El Gazouli, P. Bigenwald, and A. Joullié, "Performance simulation of 3.3 µm interband laser diodes grown on InAs substrate," Physica E **14**(4), 375–384 (2002).

#320886 https://doi.org/10.1364/OME.8.001075
Journal © 2018 Received 1 Feb 2018; revised 22 Mar 2018; accepted 25 Mar 2018; published 29 Mar 2018

Optical Materials EXPRESS

14. C. Thelander, M. R. Björk, M. W. Larsson, A. E. Hansen, L. R. Wallenberg, and L. Samuelson, "Electron transport in InAs nanowires and heterostructure nanowire devices," Solid State Commun. **131**(9–10), 573–579 (2004).
15. G. Nylund, K. Storm, S. Lehmann, F. Capasso, and L. Samuelson, "Designed quasi-1D potential structures realized in compositionally graded InAs1-xPx nanowires," Nano Lett. **16**(2), 1017–1021 (2016).
16. D. Ren, A. C. Farrell, and D. L. Huffaker, "Selective-area InAsSb nanowires on InP for 3–5 μm mid-wavelength infrared optoelectronics," MRS Advances **2**(58–59), 3565–3570 (2017).
17. S. A. Dayeh, E. T. Yu, and D. Wang, "III-V nanowire growth mechanism: V/III ratio and temperature effects," Nano Lett. **7**(8), 2486–2490 (2007).
18. A. I. Persson, L. E. Fröberg, S. Jeppesen, M. T. Björk, and L. Samuelson, "Surface diffusion effects on growth of nanowires by chemical bean epitaxy," J. Appl. Phys. **101**(3), 034313 (2007).
19. S. Paiman, Q. Gao, H. J. Joyce, Y. Kim, H. H. Tan, C. Jagadish, X. Zhang, Y. Guo, and J. Zou, "Growth temperature and V/III ratio effects on the morphology and crystal structure of InP nanowires," J. Phys. D Appl. Phys. **43**(44), 445402 (2010).
20. K. Tomioka, J. Motohisa, S. Hara, and T. Fukui, "Control of InAs nanowire growth directions on Si," Nano Lett. **8**(10), 3475–3480 (2008).
21. A. Lin, J. N. Shapiro, A. C. Scofield, B. L. Liang, and D. L. Huffaker, "Enhanced InAs nanopillar electrical transport *by in-situ* passivation," Appl. Phys. Lett. **102**(5), 053115 (2013).
22. M. Mattila, T. Hakkarainen, H. Lipasanen, H. Jiang, and E. I. Kauppinen, "Catalyst-free growth of In(As)P nanowires on silicon," Appl. Phys. Lett. **89**(6), 063119 (2006).
23. J. Treu, M. Bormann, H. Schmeiduch, M. Döblinger, S. Morkötter, S. Matich, P. Wiecha, K. Saller, B. Mayer, M. Bichler, M. C. Amann, J. J. Finley, G. Abstreiter, and G. Koblmüller, "Enhanced luminescence properties of InAs-InAsP core-shell nanowires," Nano Lett. **13**(12), 6070–6077 (2013).
24. G. Landgren, P. Ojala, and O. Ekström, "Influence of the gas switching sequence on the optical properties of ultrathin InGaAs/InP quantum wells," J. Cryst. Growth **107**(1–4), 573–577 (1991).
25. H. A. McKay, R. M. Feenstra, P. J. Poole, and G. C. Aers, "Cross-sectional scanning tunneling microscopy studies of lattice-matched InGaAs/InP quantum wells: variations in growth switching sequence," J. Cryst. Growth **249**(3–4), 437–444 (2003).
26. A. C. Farrell, W. J. Lee, P. Senanayake, M. A. Haddad, S. V. Prikhodko, and D. L. Huffaker, "High-quality InAsSb nanowires grown by catalyst-free selective-area metal-organic chemical vapor deposition," Nano Lett. **15**(10), 6614–6619 (2015).

1. Introduction

Semiconductor photonic devices operating at wavelengths longer than 2.5 μm have received increasing attention due to the variety of applications in lasers and photodetectors at mid-wavelength infrared (MWIR). To date, there has been significant effort to develop MWIR materials on InP substrates, allowing direct epitaxy of high-performance optical devices on well-studied substrates at a reduced cost compared to InAs substrates. Those optical devices include, but are not limited to, extended InGaAs interband photodetectors [1], InGaAs/InAlAs (type-I) quantum-well infrared photodetectors [2], and InGaAs/GaAsSb(Bi) (type-II) multi-quantum well lasers and photodetectors [3–6]. Another material system based on arsenic-rich InAs(Sb)/InAsP type-I heterojunctions with compressively strained InAs(Sb) layers serves as a potential candidate as well for interband optical devices with minimized Auger recombination [7,8]. However, thin film epitaxy of InAsP/InAs(Sb) heterostructures, especially with high antimony or phosphorus composition, is challenging due to lattice mismatches, which might result in planar defects. Alternatively, heteroepitaxy with large lattice mismatch can be achieved by the bottom-up growth of vertical freestanding nanowires due to elastic deformation occurring at heterogeneous interfaces [9,10].

Growth of thin film InAsP/InAs(Sb) multi-quantum well and superlattices has been previously reported for the applications of lasers and light-emitting diodes up to 6 μm, available in the literature [7,8,11–13]. On the other hand, growth of InAs/In(As)P heterostructures in nanowires has been achieved by chemical beam epitaxy to realize quasi one-dimensional potential barriers as well as quantum devices such as resonant tunneling diodes and single-electron transistors [14,15]. Unfortunately, all those heterostructures mentioned above are grown on InAs substrates, and no study in nanowires regarding optical properties of InAs(Sb) in this material system has been shown.

In this letter, we provide a detailed study of high yield axial InAs(Sb) inserts in InAsP nanowires grown on InP substrates by catalyst-free selective-area metal-organic chemical

Optical Materials EXPRESS

vapor deposition (SA-MOCVD). Selective-area growth of nanowires has been demonstrated to be a more robust technique than assembled growth, because the engineered patterns of nanowire arrays, such as periodicity, pitch, and placement, enable the exploitation of unique optical properties. Interestingly, we find that the aspect ratio of insert segments can be freely controlled by the V/III ratio during growth. Strong optical emission over 2.3 μm has been obtained from nanowire arrays with InAs(Sb) inserts at cryogenic temperature. We further examine InAs/InAsP heterointerfaces by scanning transmission electron microscope and energy-dispersive X-ray spectroscopy. These results establish an experimental foundation for engineering interband transitions and enabling hybrid integration for nanoscale MWIR optical devices.

2. Experimental details

InAs and InAsSb inserts in InAsP nanowires were grown on Zn-doped InP (111)B substrate using SA-MOCVD. Note that for SA-MOCVD, growth of vertical arsenic-rich InAs(P)(Sb) nanowires is more favorable along (111)B instead of (111)A [10]. A schematic diagram of the nanowire structure with an insert is illustrated in Fig. 1(a). To achieve high vertical yield on InP (111)B, a thin layer of InAs was introduced prior to nanowire growth [8,16]. Here, the major steps of the process are given. A 20 nm silicon dioxide (SiO_2) film was first deposited on the substrate as a growth mask, and then patterned with nanoholes by electron-beam lithography (EBL). The substrate was subsequently exposed by reactive ion etching of the SiO_2 mask. The diameter and pitch of the nanoholes were 40 nm and 600 nm, respectively. Nanowire growth was accomplished using a low-pressure (60 Torr) Emcore D-75 MOCVD reactor with hydrogen (H_2) as the carrier gas. The group III precursor was trimethylindium [TMIn], and the group V precursors were tertiarybutylphosphine [TBP], tertiarybutylarsine [TBAs], and trisdimethylaminoantimony [TDMASb]. Before nanowire growth was initialized, all samples were annealed at a temperature of 590°C for 10 minutes to fully remove the surface native oxide. The temperature was then decreased to the growth temperature at 550°C. Growth of InAs inserts was carried out at a V/III ratio between 16 and 48, while for the growth of InAsSb inserts, the V/III ratio was kept fixed at 4. A 2-sec growth interruption with H_2 purge was used as the switching sequence for all heterointerfaces. An antimony vapor phase, i.e. [TDMASb]/([TDMASb] + [TBAs]), of 0.6 was used for InAsSb inserts. Finally, the growth was terminated by shutting off TMIn, and the chamber was cooled down under TBP overpressure. Note that we intentionally induced slight overgrowth in the lateral direction during growth of the upper InAsP segment as a passivation layer for the inserts. Figure 1(b) shows a scanning electron microscope (SEM) image of a close-up look of a highly-uniform InAsP nanowire array with InAs inserts.

The height and diameter of nanowires were characterized using SEM. Photoluminescence (PL) measurement at cryogenic temperature (77 K) was carried out by a solid-state red laser at 671 nm as the pumping source (normal incidence, polarization ratio > 100:1) and a liquid-nitrogen cooled InSb detector in a Nicholet 6700 Fourier transform infrared (FTIR) spectrometer. The incident laser power and the spot size on samples were calibrated as 2 mW and 50 μm, respectively. In addition, a step-scan mode with a resolution of 32 cm^{-1} was used for FTIR. The InAs inserts were further examined by scanning transmission electron microscope (STEM) and energy-dispersive X-ray spectroscopy (EDX). To prepare the STEM/EDX samples, nanowires were mechanically moved onto the grids with carbon films.

3. Results and discussion

3.1 InAs inserts

Purely axial growth of small bandgap inserts is desired for nanowires because any overgrowth in the lateral directions may form a shunt path for carriers through the spacing between segments. Thus, the first part of the study concerns the growth condition to achieve a high

Optical Materials EXPRESS

aspect ratio, i.e. nanowire height divided by nanowire diameter, with enhanced axial growth and eliminated lateral growth. Interestingly, we observe that by tuning V/III ratio the aspect ratio can be freely controlled. As shown in Fig. 2(a), three different V/III ratios of 16, 32, and 48 are applied to 30-sec growth of InAs inserts on top of InAsP bottom segments, which results in very different nanowire dimensions. The changes of height and diameter after InAs growth are characterized by SEM and summarized in Fig. 2(b), and the calculated aspect ratio as a function of V/III ratio is shown in the inset. The results are remarkable – an aspect ratio of nearly 100 is achieved using a V/III ratio of 16, meaning that growth of a 100 nm axial InAs insert only results in a lateral overgrowth of about four monolayers on nanowire sidewalls. The increase of aspect ratio with decreasing V/III ratio can be explained by a lower activation energy at the InAsP/InAs interface due to precursor pyrolysis [17] or interpreted by an enhanced diffusion length of indium adatoms on SiO_2 growth mask due to less phosphorus [18,19].

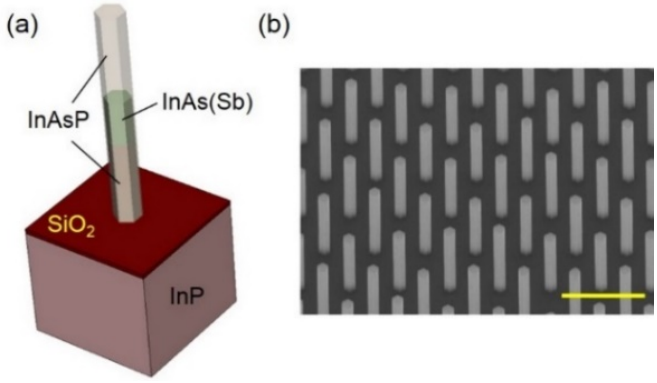

Fig. 1. (a) Schematics of InAs(Sb) inserts in InAsP nanowires grown on InP (111)B. (b) A close-up look of nanowire array with InAs inserts. The scale bar is 1 μm.

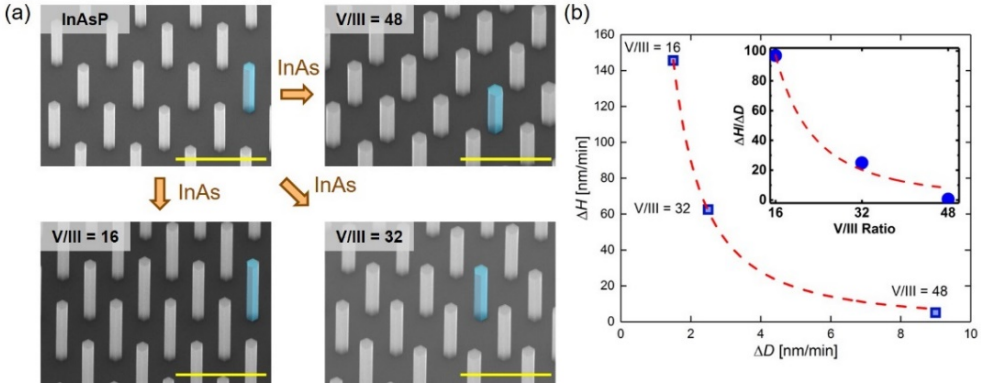

Fig. 2. (a) SEM images of InAs segments grown on InAsP bottom segments using different V/III ratios of 16, 32, and 48. The scale bar is 1 μm. (b) The average change of nanowire height ΔH as a function of the average change of nanowire diameter ΔD after the growth of InAs inserts. The inset shows the aspect ratio of InAs growth as a function of V/III ratio.

PL characterization of InAsP/InAs/InAsP heterostructures (shown in Fig. 1(a)) is carried out at cryogenic temperature (77 K), as shown in Fig. 3(a). The growth time of InAs inserts is varied from 5 to 30 seconds. The emission peak at lower energy is attributed to the emission from InAs inserts, shaded in blue, which spans a wavelength range of 2.31 – 2.57 μm, while the peak at a higher energy results from InAsP segments. Spectrum fitting is accomplished by using only two Gaussian functions, suggesting interband transitions are the dominant form of emission for all segments. The peak energy of InAs inserts as a function of growth time is

Optical Materials EXPRESS

displayed in Fig. 3(b). We observe that the peak energy of InAsP segments is almost constant between 0.630 and 0.635 eV, while the peak energy of InAs inserts shifts towards higher energy with decreasing growth time. The phosphorus composition is estimated to be 0.23 and 0.24 based on our previous growth study of InAsP nanowires on InP substrates [10]. The peak shift of InAs inserts might result from phosphorus inter-diffusion at InAsP/InAs heterointerfaces, or the quantized well-like structure of InAs. Additionally, it is noted that the emission peak of InAs inserts grown for 30 seconds is at 0.483 eV, much different from the zinc-blende InAs bandgap of 0.415 eV at 77 K. It is mainly due to a high-density of rotational twins, i.e. crystal phase switches between zinc-blende and wurzite, which is commonly observed in InAs nanowires grown by selective-area growth mode [20,21].

Having determined the peak energy, we study the surface passivation for InAs inserts. As mentioned earlier, top InAsP segments are intentionally grown laterally to realize passivation layers with larger bandgap. It is known that by introducing phosphorus into InAs the surface state density can be largely suppressed [10,22,23]. Here, we compare the PL emission from two nanowire arrays with 30-sec and 60-sec InAsP top segments while the growth time of InAs inserts is kept fixed at 30 seconds. The measured PL spectra are depicted in Fig. 3(c). As expected, the emission from inserts is enhanced by a factor of seven with no shift of InAs peak energy. Thus, it is evident that the increased emission results from a reduction of surface state density at nanowire surface.

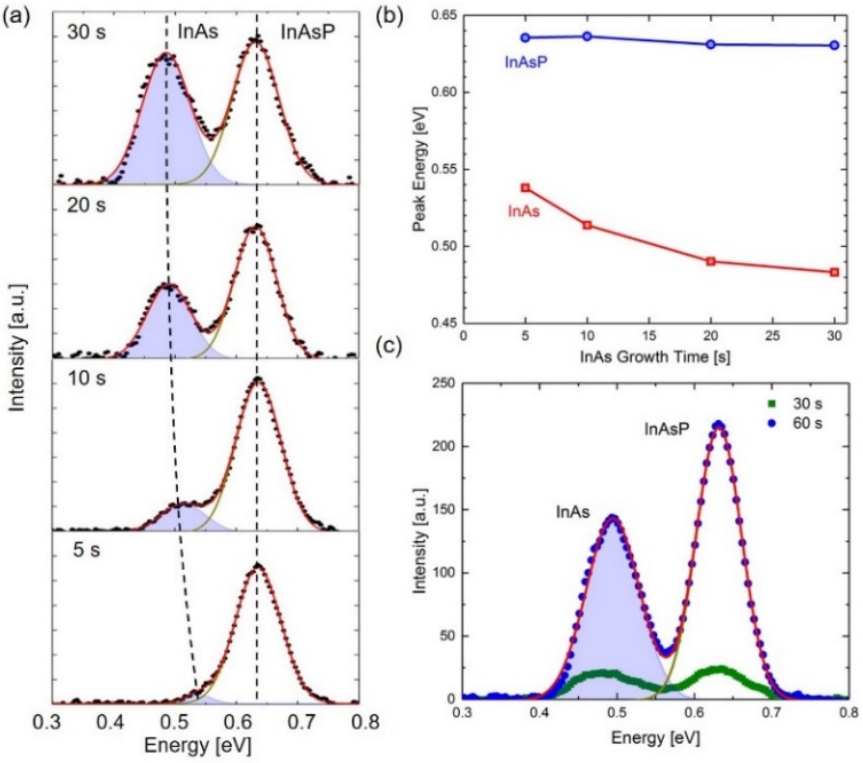

Fig. 3. (a) PL characterization (77 K) of nanowire arrays with InAs inserts. The growth time of inserts is varied from 5 to 30 seconds. The dashed lines are drawn to guide the eye for the emission peaks of InAs and InAsP segments. (b) A summary of peak energy as a function of growth time of InAs inserts. (c) Optical emission of nanowire arrays where the InAsP top segments are grown for 30 and 60 seconds, respectively. The growth time of InAs inserts is kept fixed at 30 seconds.

Optical Materials EXPRESS

Figure 4 shows STEM/EDX characterization of a single nanowire with a 60-sec InAs insert. The insert is clearly shown in the highlighted region with an estimated width of 150 nm. In this study, we use a 2-sec H_2 purging scheme during growth interruptions between segments as the source gas switching procedure. The duration of H_2 purging is critical – the residual arsenic or phosphorus adatoms need to be fully removed to avoid being incorporated into the next growth segment. This is normally known as the "memory effect" for As/P material systems [24,25]. One potential solution is to optimize the switching sequence of As/P by extending the time of H_2 purging scheme to fully remove any residual arsenic or phosphorus adatoms on dielectric growth masks. Since the EDX measurement was performed on an as-grown nanowire (no thinning), the scan resolution is insufficient to accurately assess the abruptness of the heterointerface and so further study will be necessary.

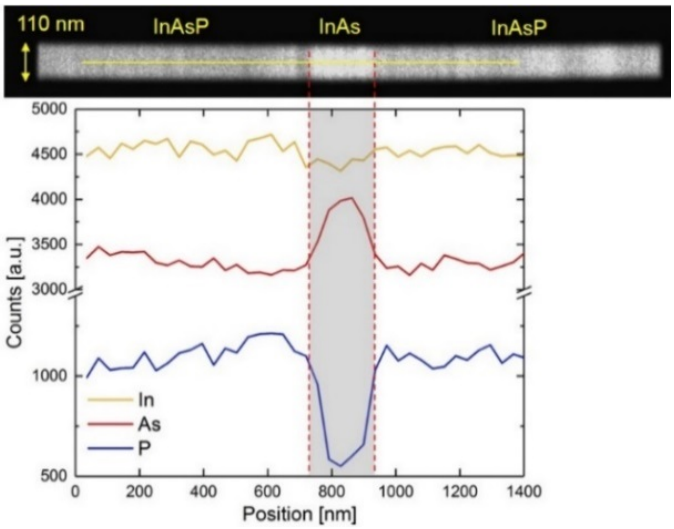

Fig. 4. STEM and EDX line-scan of a single nanowire with a 60-sec InAs insert.

3.2 InAsSb inserts

We now present a study of InAsSb inserts in InAsP nanowires. Growth of purely axial InAsSb inserts is achieved using a V/III ratio of 4, as shown in Fig. 5(a). The axial growth rate of InAsSb is determined to be 282 nm/min. Similar to the previous growth of InAs inserts, the top InAsP segments are used as high bandgap passivation layers. We performed 77 K PL measurements of as-grown samples of InAsP/InAsSb and InAsP/InAsSb/InAsP, as shown in Fig. 5(b) and 5(c), respectively. In Fig. 5(b), the emission peak of InAsSb, shaded in blue, is at 0.390 eV, i.e. 3.12 μm. It is not surprising that there is no InAsP emission in the spectrum and the signal from InAsSb nanowires is weak. First, an exchange of arsenic and phosphorus on nanowire surface occurs during InAsSb growth, resulting in an arsenide-like surface with high density of surface states for the bottom InAsP segments [10]. Second, the weak InAsSb emission is due to a high surface state density as well. By adding the top InAsP segments, inserts and bottom InAsP segments are properly passivated, and thus, the emission from both inserts and InAsP segments are dramatically enhanced, as shown in Fig. 5(c). We note that the peak energy of InAsSb is shifted from 0.390 eV to a lower energy of 0.335 eV (3.70 μm), which results from a relaxation of Fermi-level pinning at the surface of InAsSb inserts. The antimony composition is estimated to be between 0.08 and 0.10 based on previous growth studies of InAsSb nanowires [16,26]. Additionally, the full-width half-max (FWHM) of the InAsSb peak is 73.7 meV, higher than the value obtained from InAsSb bulk nanowires, which is about 45.0 meV [26]. This might be due to a nonuniform antimony composition across the insert segment.

Optical Materials EXPRESS

4. Conclusion

We successfully grew InAs and InAsSb inserts in InAsP nanowires on InP (111)B substrates by SA-MOCVD. We observed optical emission spanning a wavelength range from 2.31 – 3.70 µm from interband transition by PL characterization. The growth of InAs inserts was further examined by STEM/EDX. It is worth noting that by choosing a proper V/III ratio, we achieved the growth of inserts with high aspect ratio. We believe that this study provides a promising approach to integrate InAs(Sb) active layers on low-cost InP substrates for optoelectronics at MWIR.

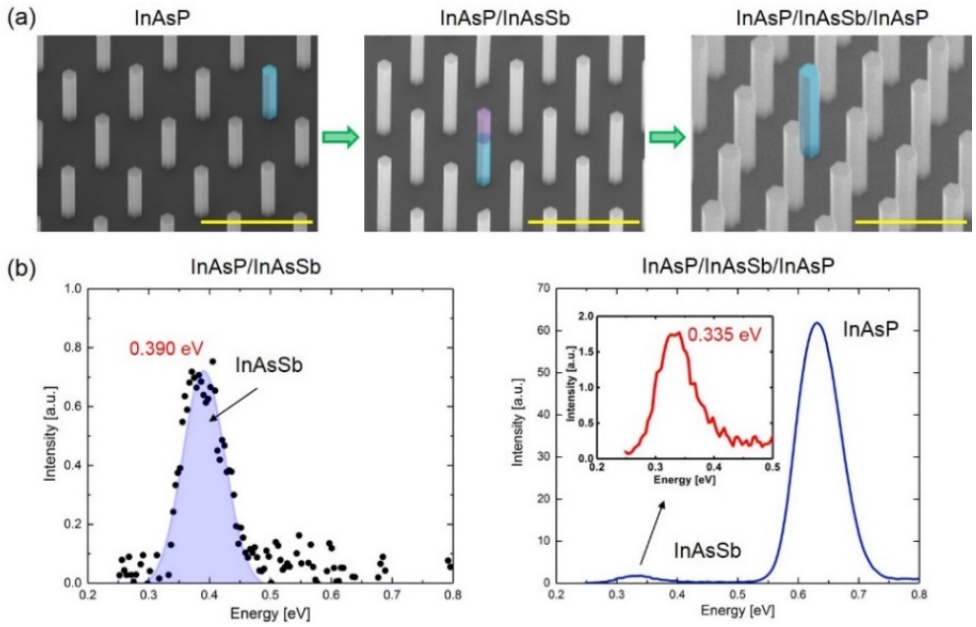

Fig. 5. (a) SEM images of growth process of InAsSb inserts. (b) PL characterization (77 K) of InAsP/InAsSb and InAsP/InAsSb/InAsP heterostructures, respectively. The inset shows a close-up look of emission from InAsSb inserts.

Funding

National Science Foundation (NSF) (ECCS-1509801); Sêr Cymru National Research Network in Advanced Engineering and Materials.

Acknowledgments

We acknowledge the user facilities at UCLA – Nanoelectronics Research Facility as well as Integrated Systems Nanofabrication Cleanroom (ISNC), and Electron Imaging Center for NanoMachines (EICN) in California NanoSystems Institute (CNSI). We also gratefully acknowledge the financial support for this research from the National Science Foundation (grant no. ECCS-1509801) and Sêr Cymru National Research Network in Advanced Engineering and Materials.